Discovery of Non-Thermal X-Rays from the Shell of RCW 86

Aya Bamba, Katsuji Koyama[1]
Department of Physics, Graduate School of Science, Kyoto University, Sakyo-ku, Kyoto 606-8502
E-mail(AB): bamba@cr.scphys.kyoto-u.ac.jp
and
Hiroshi Tomida
National Space Development Agency of Japan,
World Trade Center Bldg, 2-4-1 Hamamatu-cho,Minato-ku, Tokyo,105-8060

arXiv:astro-ph/0007365v2 16 Aug 2000

We report the ASCA (Advanced Satellite for Cosmology and Astrophysics) results of RCW 86, a shell-like supernova remnant (SNR). The bright region in the X-ray band traces the radio clumpy shell, although details of the structure are different. The X-ray spectrum from each part of the shell can not be fitted to a thin thermal plasma model, but requires, at least three components: a low temperature plasma of 0.3 keV, high temperature plasma of $\geq$ several keV, and a power-law component with a photon index $\sim$ 3. The abundances of O, Ne, Mg and Si are significantly higher than that of Fe, indicating that RCW 86 is a type II SNR. The absorption column of $\sim 3\times 10^{21}$ H cm^{-2} indicates the distance to the SNR to be several kpc. The power-law component can be interpreted to be synchrotron radiation of high energy electrons. Assuming energy density equipartition between the magnetic field and the electrons, and using the radio and X-ray spectra, we argue that high energy electrons are accelerated up to 20 TeV. The acceleration efficiency is, however, different from shell to shell.

Key Words: acceleration of particles — supernova remnants: individual(RCW 86) — X-rays: ISM

1 Introduction

The origin and acceleration of cosmic rays have been a long-standing key problem since the discovery in 1911-1912 (Hess 1911; Hess 1912). The energy spectrum of cosmic rays is presented by a power-law function with a break at $\sim 10^{15.5}$ eV called "knee energy". The presence of the break in the power-law distribution indicates that cosmic rays may have two different origins. A natural explanation is that cosmic rays below the knee energy are originated in our Galaxy, while those above the knee are extragalactic origin. The most probable origin and acceleration mechanism of the Galactic cosmic rays are the first order Fermi acceleration process by fast moving shells of supernova remnants (SNRs) (Wentzel 1974). In fact, radio spectra and polarizations in SNR shells are well represented by synchrotron radiations of high energy electrons with a power-law distribution of an index expected from the Fermi acceleration process. The radio data thus indicate that GeV energy electrons are accelerated in SNR shells.

If electrons are accelerated to a higher energy near the knee, the energy of synchrotron radiation shifts to an X-ray band. Shell-like SNRs, however, typically display line-dominated thermal X-rays, with the characteristic temperature of about 1 keV, due to either a single or multi-components plasma. Thus no evidence for synchrotron X-rays has been so far found. Recently two shell-type SNRs, SN 1006 and G347.3−0.5 are found to be dominated by power-law X-rays with no emission line (Koyama et al. 1995; Koyama et al. 1997; Slane et al. 1999). The power-law X-rays, together with the discoveries of TeV gamma rays (Tanimori et al. 1998, Muraishi et al. 2000), have indicated that the shell of these SNRs are the acceleration sites of extremely high energy electrons of 10^{13} to 10^{15} eV. In such relativistic energy, protons, the main component of cosmic rays, and electrons are essentially the same except for the charge polarity (Bell, 1978). Therefore, these two SNRs are most probable sites of cosmic ray accelerations near to "knee energy".

Some hints for synchrotron X-rays from other shell-like SNRs are found with ASCA (Advanced Satellite of Cosmology and Astrophysics), RXTE (Rossi X-ray Timing Explorer) and CXO (Chandra X-ray Observatory). Even typical thin thermal SNRs, such as Cas A, IC443, Tycho, Kepler, G156.2+5.7 and RCW 86 exhibit hard energy tails over the thin thermal emissions. Some of the hard tails are most likely to be non-thermal (Cas A and IC443; Petre et al. 1997), but the others are controversial, either non-thermal or higher energy plasma of about 10 keV. Since high energy particles from a higher temperature plasma (e.g. $\geq$

[1]CREST, Japan Science and Technology Corporation (JST), 4-1-8 Honmachi, Kawaguchi, Saitama 332-0012 JAPAN

10 keV) are more easily injected into the "Fermi acceleration machine" than those from a lower temperature plasma (e.g. $\sim$ 1 keV) (Bell, 1978), it is essentially important to investigate the relation of high energy plasma and non-thermal emission.

RCW 86 was identified as the remnant of the historical supernova in A.D.185 (Clark and Stephenson 1977). However Chin and Huang (1994), and Schaefer (1995), derive the age of RCW 86 to be $\sim$ 8000 yrs with a Sedov solution. Since RCW 86 is located in an OB star association, it is likely to be a type II SNR (Clark and Stephenson, 1977). X-rays from RCW 86 were discovered by Naranan et al. (1977). The X-ray spectrum obtained with the Einstein satellite was represented by a two-temperature plasma model (Winkler 1978). The higher energy spectrum (2.0–20 keV) with the Ginga satellite was explained by a single temperature plasma of $kT \geq 4$ keV (Kaastra et al. 1992). Using the ASCA satellite, Vink et al. (1997) reported that the plasma temperature varies from region to region of the shells, from 0.8 keV to > 3 keV. Petre et al. (1999) found a hard X-ray tail extending to several 10 keV in the RXTE spectrum. They thus argued that the shell of RCW 86 has a non-thermal emission and is one of the candidate for the origin of high energy cosmic rays. However, non-imaging instrument of RXTE could not make clear which region of the SNR is the hard X-ray emitter. In this paper, we revisit to the ASCA data and examine whether or from which region is RCW 86 emitting non-thermal hard X-rays.

2 Observations

RCW 86 was observed with ASCA (Tanaka et al. 1994) on 1993 August 17-18. X-ray photons are collected with four XRTs (X-Ray Telescopes; Serlemitsos et al. 1995) and detected with two SIS (Solid-state Imaging Spectrometers; Burke et al. 1991) cameras and two GIS (Gas Imaging Spectrometers; Ohashi et al. 1996) on the foci of the XRTs. Three mosaic observations have been conducted, because the size of RCW 86 is larger than the field of view of SIS. The SISs were operated in 4-CCD read-out mode, with the data acquisition of faint mode in the High bit rate and bright mode in the Medium and Low bit rates. No significant degradation is found in the SIS data taken about 6 months after the launch, hence no correction for the Residual Dark Distribution (RDD) is required (T. Dotani et al. 1997, ASCA News 5, 14). The GISs were operated in the normal PH mode. We excluded high-background data and non X-ray events with the standard method according to the user guide by NASA Goddard Space Fright Center. Then, the available exposure times are $\sim$ 20 ks, $\sim$ 9 ks, and $\sim$ 8 ks, for each observation.

3 Analyses and Results

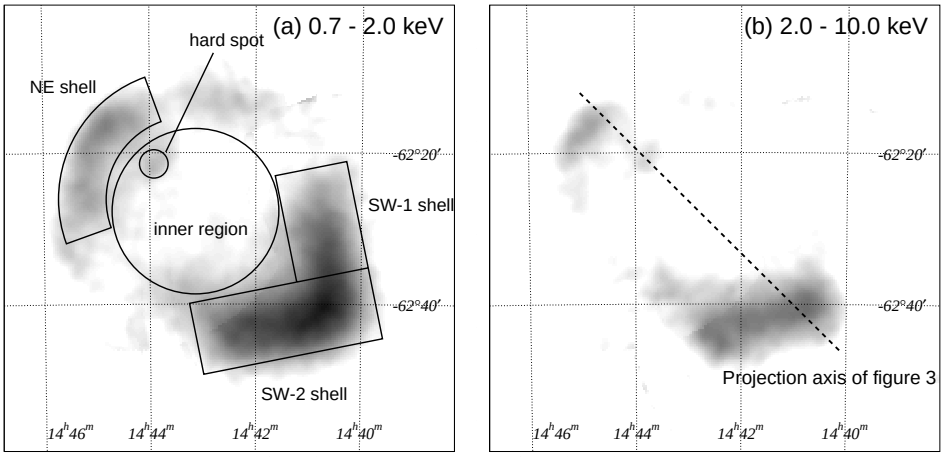

Figure 1: Mosaic GIS maps in the 0.7–2.0 keV (a) and the 2.0–10.0 keV (b) bands with J2000 coordinate. Vignetting and exposure time have been corrected. The gray map is drawn in logarithmic scale.

Figure 1 shows the GIS mosaic images around RCW 86 in the energy bands of 0.7–2.0 keV (figure 1a)

and 2.0–10.0 keV (figure 1b), in which vignetting and exposure times are corrected. In both the images, we can see two prominent shells at northeast and southwest of the RCW 86 rim. The sizes and shapes of the X-ray shells are similar to those of Hα (Smith 1997) and the 847 MHz band (Kesteven and Caswell 1987). With a quick look, we see different structure between the two energy bands, or the spectrum is different from region to region. In the 0.7–2.0 keV band, the southwest shell is appeared to be boomerang shape, while in the 2.0–10.0 keV band, the shell changes to bar-like structure. The northeast shell is brighter in the hard band than in the soft band. We also detected a point-like spot near the northeast shell in figure 1a with a significance of 4σ.

We made the X-ray spectra from each region with the designation given in figure 1a. Since RCW 86 is located near on the Galactic plane, contamination from the Galactic ridge plasma emission can not be ignored (Koyama et al. 1987). Hence the background spectrum is taken from outside of RCW 86 but near the same Galactic latitude as the source region, and is subtracted from the source spectrum. We first made the spectra from the brightest shell, SW shell (combined with SW-1 and SW-2 shells). Although we treated both the GIS and SIS spectra simultaneously to increase statistics, we show, for simplicity, only the SIS spectrum in figure 2a. Prominent emission lines from highly ionized O, Ne, Mg, Si and Fe atoms in the spectrum imply that significant fraction of the X-rays is attributable to a thin thermal plasma. Therefore, we applied a thin thermal model in non-equilibrium ionization (Masai 1984) as was already tried by Vink et al. (1997). This model is statistically rejected with $\chi^2 = 2154/685$, even the abundances of O, Ne, Mg, Si and Fe are allowed to be free parameters. Large residuals are found in the 1–2 keV and above 5 keV bands. We note that the thermal model reported by Vink et al. (1997) is unacceptable to our GIS and SIS simultaneous fitting. In fact, the iron K-shell line and those from lighter elements such as O, Ne, Mg and Si can hardly coexist in a single temperature plasma. We thus added another higher temperature thin plasma in non-equilibrium ionization. This two-temperature plasma model is still rejected with $\chi^2 = 1685/682$. Significant data excess is found at high energy continuum above 6.5 keV. The discrepancy of the model and data become larger in higher energy. In fact, this model spectrum can only account 10% of the RXTE flux at > 10 keV reported by Petre et al. (1999).

Accordingly, we are required to add a non-thermal (power-law) component, hence applied a model consisting with two thin thermal plasmas component 1 (dotted line) and 2 (dashed line), respectively, and a power-law component (solid line, see figure 2a). For simplicity, the absorption column is taken to be common among the three components, and the abundances of O, Ne, Mg, Si, and Fe in component 1 and that of Fe in component 2 are allowed to be free parameters, while the others are fixed to be solar values (Allen 1973). χ^2 is then greatly reduced to be marginally value of 979/682. Therefore we do not try more complicated models, although this 3-component model is still rejected in a statistical point of view. The best-fit parameters are shown in table 1.

The power-law fluxes extrapolated to higher than 10 keV are smoothly connected to the RXTE results as is shown in the best-fit model function given in figure 2b. Thus the hard X-rays obserevd with RXTE can be regarded to be a higher energy part of the power-law component found with the present ASCA analysis of the brightest shell.

For the diffuse spectra from the other regions of this SNR, we applied the same model as SW shell, allowing only the normalizations of the three components and the ionization parameter to be free, otherwise the limited photon statistics of these faint regions give no essential constraint on the physical parameters. This simplified model approach is found to be reasonable, because the reduced χ^2 for the fitting of each region is about 1.5–1.8, comparable to that in the SW shell analysis. The best-fit ionization parameters, fluxes and the flux ratios for each component are shown in table 2.

Figure 3 is a projected profile of RCW 86 to the dotted line given in figure 2b. We can clearly see a hard spot near the NE shell, with the width of about $3'$, corresponding to the spatial resolution of GIS. We thus regard the hard spot to be a point source. The spectrum of the hard spot is taken from a circle of $3'$ radius on the source, and that of the background is an annulus region of $3'$–$6'$ radius around the source. The background subtracted spectrum shows no significant line, and can be fitted to a power-law model of a photon index $= 2.3^{+0.2}_{-0.2}$ and absorption of $N_{\rm H} = 2.0^{+0.9}_{-0.8} \times 10^{21}{\rm cm}^{-2}$ with reduced $\chi^2 = 51/70$ (here and after, errors are 90 % confidence). The total flux in the 0.7–10.0 keV band is 3.7×10^{-12}erg cm^{-2}s^{-1}.

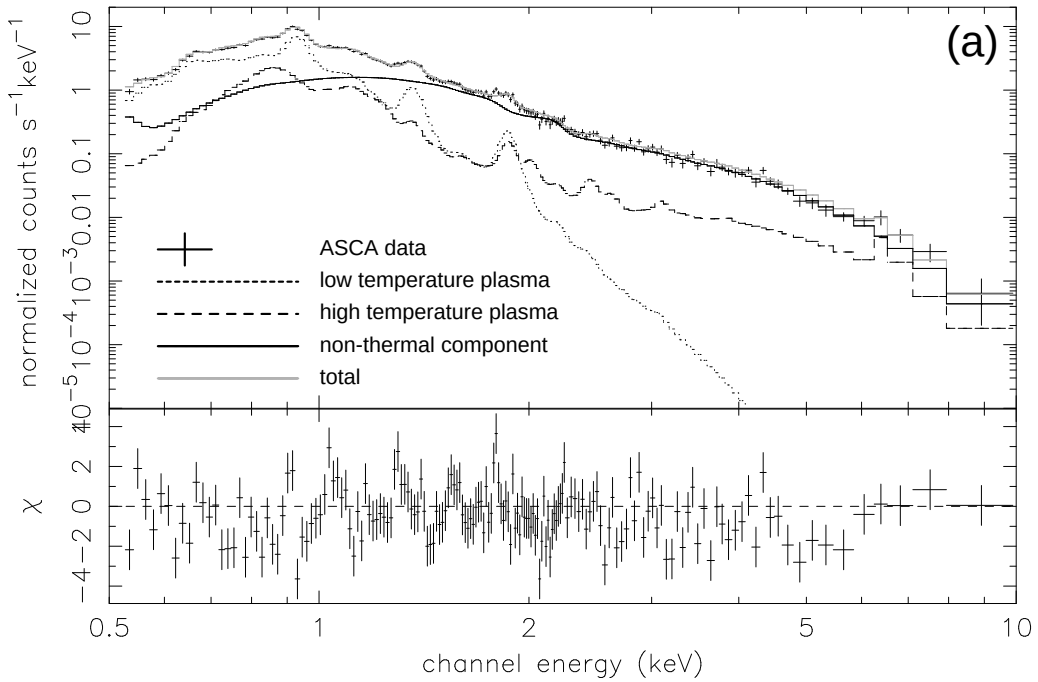

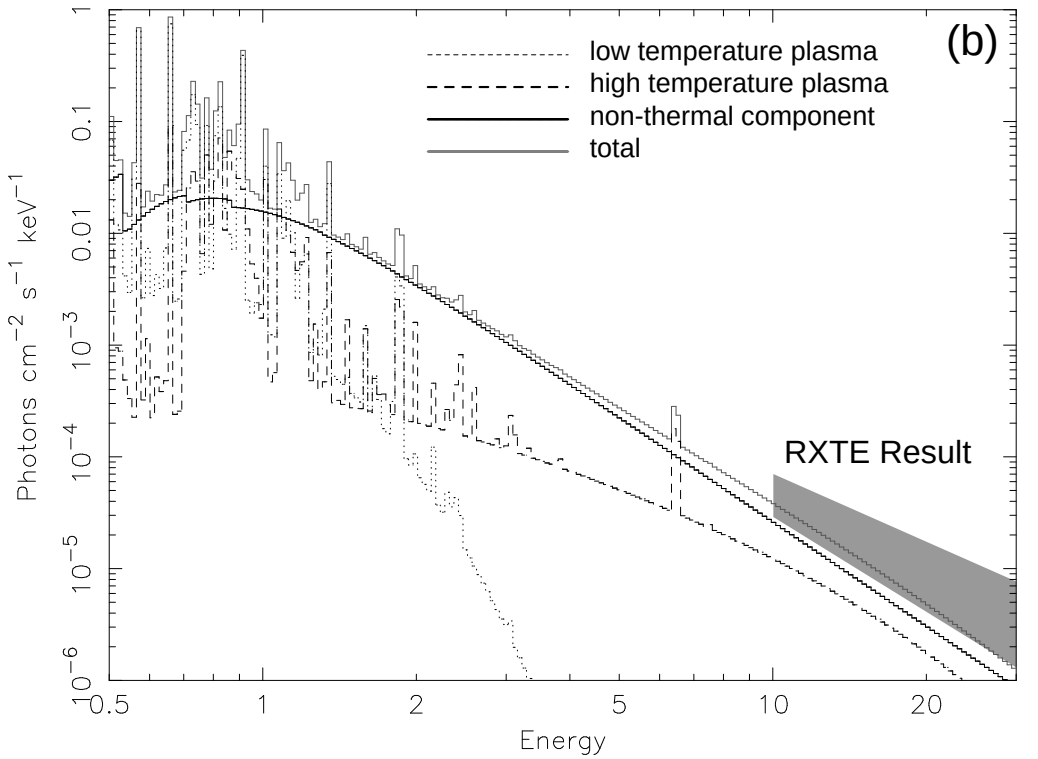

Figure 2: (a) The ASCA SIS 0+1 spectra from SW shell of RCW 86 with the best-fit models (upper panel). Residuals from the best-fit models are shown in the lower panel. The dotted, dashed, and solid line represents the best-fit models(see text). (b) The photon flux of the best-fit model. The hatched area represents the photon fluxes and errors with the RXTE observations.

Table 1. Best-fit parameters for SW shell for a two-temperature plasma and power-law model.*

Parameters	Component 1	Component 2	Non-thermal component
kT (keV)	0.34 (0.30 – 0.38)	23.8 (15.1 – 26.0)	···
$\log nt$ (s cm^{-3})	10.7 (10.6 – 10.8)	10.1 (10.0 – 10.2)	···
O/H†	3.3 (2.3 – 3.8)	···	···
Ne/H†	(> 6.7)	···	···
Mg/H†	(> 4.7)	···	···
Si/H†	(> 6.5)	···	···
Fe/H†	2.4 (1.7 – 3.1)	3.3 (2.3 – 6.0)	···
photon index	···	···	3.1 (3.0 – 3.2)
$N_{\rm H}$ ($\times 10^{21}$ H cm^{-2})	3.2 (2.9 – 3.8)	3.2‡	3.2‡
Flux (erg cm^{-2} s^{-1})§	1.5E−10	6.2E−11	1.0E−10

* Parentheses indicate 90 % confidence regions for one relevant parameter.
† Abundance ratio relative to the solar value.
‡ Common with component 1.
§ In the 0.7–10.0 keV band.

4 Discussions

We found that the X-ray spectra of RCW 86 have three components; a lower temperature plasma (component 1), higher temperature plasma (component 2), and a power-law emission (non-thermal component). Since the abundance of light elements such as O, Ne, Mg, and Si are higher than that of Fe, RCW 86 is likely due to a type II SN, consistent with that RCW 86 is in an OB star association (Clark and Stephenson 1977). The best-fit column density of 3.2×10^{21} H cm^{-2} is also consistent with the distance to the OB star association of 2.5 kpc. Here and after, we adopted this value for the distance to RCW 86. The discovery of the hard spot in RCW 86 is also suggestive for the Type II concept. We separately discuss for these emissions.

4.1 Hard Spot

Since the absorption column of the hard spot is similar to that of SW shell, we infer that the hard spot is located in the SNR. The total luminosity is then estimated to be 2.7×10^{33} erg s^{-1}. This luminosity and the power-law spectrum of a photon index ($\alpha = 2.3$) suggest the hard spot could be a Crab-like pulsar, supporting for a type II SN origin. We therefore search for coherent pulsations using the FFT technique, however we found no hint of pulsation in the time scale of 7.825×10^{-3} sec to 16381 sec. Obviously, further sensitive searches for coherent pulsations are required.

4.2 Higher Temperature Plasma

The nature of component 2 is puzzling because the temperature of $\geq$ 10 keV is unusually high for SNRs. The presence of this high temperature plasma mainly rely on the line features around 6.5 keV, because the continuum emissions above a few keV are not sensitive to separate a high temperature plasma and a power-law emission. Thus to investigate the origin of the line feature is essentially important. Since the observed line energy is about 6.5 keV, near the K-shell transition energy of neutral or low ionization iron atoms, one may argue that the line is fluorescence from cold iron, like in a molecular cloud Sgr B2 (Murakami et al. 2000). This possibility can be rejected because the column density is too small to emits such strong neutral iron lines by the reflection mechanism. Strong iron lines from rather low ionization atoms are also found in other young SNRs, for example, Tycho and Kepler's SNRs (Hwang and Gotthelf 1996). Borkowski and Szymkowiak (1997) suspected that these iron lines in young SNRs are the composite of lines from a hot plasma and fluorescent lines coming from dust grains. If this is the case of RCW 86, the energy of iron line due to a hot plasma can be higher, then the ionization parameter become larger. Hence the true temperature

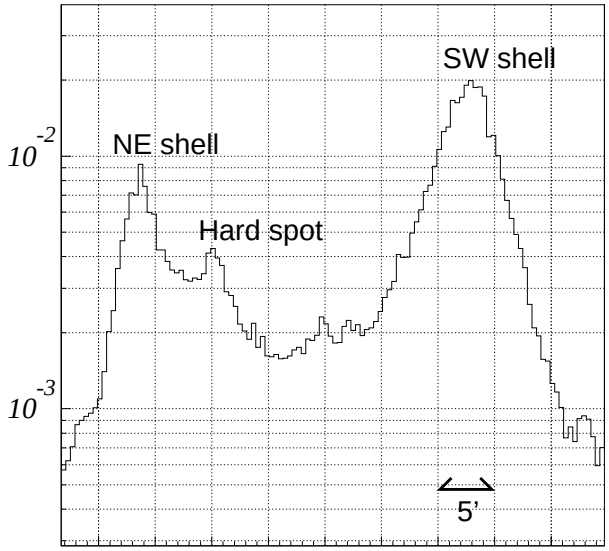

Figure 3: The projected profile to the axis given in figure 2b). The vertical axis represents count rate per bin.

of the hot plasma should be lower than 10 keV, probably around several keV, which is not unusually high for a young SNR.

4.3 Lower Temperature plasma

At the distance of 2.5 kpc, the radius of the shell (R) is estimated to be 14 pc. Assumption that SW shell covers $\pi/2$ str (see figure 1) and that the thickness is $1/12R$ (expected from Sedov solution), the density and ionization age of SW shell are estimated from the luminosity and the ionization parameter nt, to be 0.45 (0.40–0.50) cm^{-3} and 3100 (2500–3700) yr, respectively. For NE shell, we assume the covering solid angle to be $\pi/4$ str (see figure 1) and estimate the density and ionization age to be 0.06 (0.04–0.08) cm^{-3} and 1800 (1000–3900) yr, respectively. These ionization ages are significantly shorter than the Sedov age of 8000 yr (Chin and Huang, 1994; Schaefer, 1995), and favor that RCW 86 is the remnant of AD 185 (Clark and Stephenson 1977). We note that systematical difference between the ionization age and the Sedov age is found in some other Type II SNRs by Hughes et al. (1998). They have systematically analyzed shell-like SNRs in the Large Magellanic Cloud and found some of the Type II candidates shows the ionization ages shorter than the Sedov ages. They interpret that these Type II SNRs exploded within pre-existing low-density cavities in the interstellar medium. The low interior density allows the SN blast wave to propagate rapidly to the cavity wall, where it then encounters denser gas, begins to slow down, and emits copious amounts of X-rays. This scenario reduces the dynamical ages from that inferred with the Sedov model (Sedov ages). RCW 86 may be the same case, because it is likely a Type II in an OB star association (Clark and Stephenson 1977). Thus the real age would be similar to the ionization age of 3100 yr.

4.4 Power-law Emission

Figure 4 is the wide band spectrum from RCW 86, in which the radio data is refereed from Green (1998). The spectrum can be explained by a power-law model with a break at $\sim 2 \times 10^2$ eV. This break is produced by synchrotron energy loss, which is larger for higher energy electrons, hence gives the maximum electron energy. The synchrotron energy loss is proportional to the square of the magnetic field. The magnetic field is calculated using the IRAS result by Greidanus and Storm (1990) to be 80 μG under the assumption of energy equipartition. We then estimate the highest energy of electrons which have been accelerated in the shell of RCW 86 to be $\sim$ 20 TeV. Actually, many SNRs have smaller magnetic field than that on the assumption of energy equipartition. Therefore, the highest energy of electrons may be higher than our estimation.

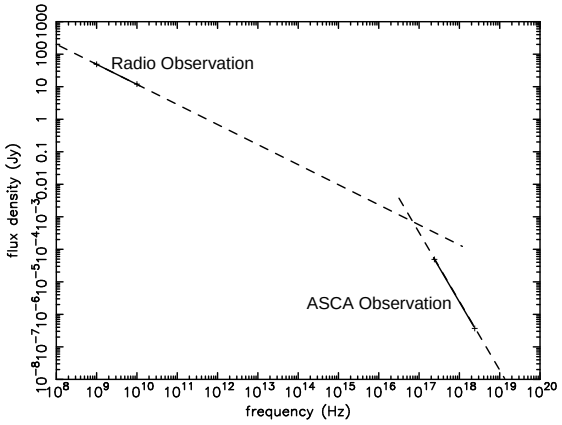

Figure 4: The wide band spectrum from radio to X-ray band. The solid lines mean observational flux density, whereas the dashed lines are extrapolated flux.

Table 2. Normalized flux of each region for the thermal and non-thermal components.*

Region	thermal component (erg s^{-1} cm^{-2} $arcmin^{-2}$) component 1	component 2	non-thermal component (erg s^{-1} cm^{-2} $arcmin^{-2}$)	N/T†	reduced χ^2
SW-1 shell	6.9E−13	1.6E−13	8.9E−14	0.1	520.5905/291
SW-2 shell	5.1E−13	2.3E−13	4.2E−13	0.6	1056.154/673
NE shell	2.5E−14	3.1E−14	1.8E−13	3.2	409.3046/256
Inner region	3.2E−16	4.3E−14	5.8E−14	1.3	135.1856/85

* In the 0.7–10.0 keV band.
† Flux ratio of the non-thermal to the thermal (component 1 + component 2).

The flux ratio of the non-thermal to thermal components is different from region to region. The thermal component is dominant in SW-1 shell, while SW-2 shell has both components. In NE shell, the non-thermal component is dominated. Both components are dim in the inner region, supporting that the non-thermal X-rays do not come from a pulsar nebula. These differences would be related to the difference of the shock intensities, the magnetic fields, and/or field line direction relative to that of the shock propagation. To address these issues, we need much higher spatial resolution instruments in the hard energy band, such as Chandra and Newton.

Note added in proof
After completing this draft, we have become aware of a pre-print by Borkowski et al. (astro-ph/0006149), which gives essentially the same conclusion with different approach of data analysis.

We are grateful to all members of the ASCA team. Our particular thanks are due to K. Yoshita for fruitful comments and suggestion about NEI models.

References

[1] Allen C.W. 1973, Astrophysical Quantities 3rd Edition (The Athlone Press, University of London)p30

[2] Bell, A.R., 1978, MNRAS 182, 147

[3] Borkowski, K.J., Szymkowiak, A.E. 1997, ApJ 477, L49

[4] Burke, B.E., Mountain, R.W., Harrison, D.C., Bautz, M.W., Doty, J.P., Ricker, G.R., Daniels, P.J. 1991, IEEE Trans. ED-38, 1069

[5] Chin, Y.N., Huang Y.N. 1994, Nature 371, 398

[6] Clark, D.H., Stephenson, F.R. 1977, The Historical Supernova (Elmsford, N.Y., pergamon)p83

[7] Dotani, T., Yamashita, A., Ezuka, H., Takahashi, K., Crew, G., Mukai, K., the SIS team 1997, ASCA news 5, 14

[8] Green D. A., 1998 'A Catalogue of Galactic Supernova Remnants (1998 September version)', Mullard Radio Astronomy Observatory, Cambridge, United Kingdom
(available on the World-Wide-Web at "http://www.mrao.cam.ac.uk/surveys/snrs/").

[9] Greidanus, H., Storm, R.G. 1990, A&A 240, 385

[10] Hess, V.F. 1911, Phys. Zeits 12, 998

[11] Hess, V.F. 1912, Phys. Zeits 13, 1084

[12] Hwang, U., Gotthelf, E.V. 1996, ApJ 475, 665

[13] Hughes, J.P., Hayashi, I., Koyama, K. 1998, ApJ 505, 732

[14] Kaastra, J.S., Asaoka, I., Koyama, K., Yamauchi, S. 1992, A&A 264, 654

[15] Kesteven, M.J., Caswell, J.L. 1987, A&A 183, 118

[16] Koyama, K., Makishima, K., Tanaka, Y., Tsunemi, H. 1986 PASJ 38, 121

[17] Koyama, K., Petre, R., Gotthelf, E.V., Hwang, U., Matsuura, M., Ozaki, M., Holt, S.S. 1995, Nature 378, 255

[18] Koyama, K., Kinugasa, K., Matsuzaki, K., Nishiuchi, M., Sugizaki, M., Torii, K., Yamauchi, S., Achenbach, B. 1997, PASJ 49, L7

[19] Masai, K. 1984 A&SS, 98, 367

[20] Muraishi, H., Tanimori, T., Yanagita, S., Yoshida, T., Moriya, M., Kifune, T., Dazeley, S.A., Edwards, P.G. et al. 2000, A&A 354, L57

[21] Murakami, H., Koyama, K., Sakano, M., Tsujimoto, M., Maeda, Y. 2000, ApJ 534, 283

[22] Naranan, S., Shulman, S., Yentis, D., Fritz, G., Friedman, H. 1977, ApJ 213, 53

[23] Ohashi T., Ebisawa K., Fukazawa Y., Hiyoshi K., Horii M., Ikebe Y., Ikeda H., Inoue H. et al. 1996, PASJ 48, 157

[24] Petre, R., Keohane, J.W., Gotthelf, E.V., Hwang, U., Allen, G., Koyama, K., Ozaki, M. 1997 IAUS

[25] Petre, R., Allen, G.E., Hwang, U. 1999, Astronomische Nachrichten 320, 199

[26] Serlemitsos P.J., Jalota L., Soong Y., Kunieda H., Tawara Y., Tsusaka Y., Suzuki H., Sakima Y. et al. 1995, PASJ 47, 105

[27] Schaefer, B.E. 1995, AJ 110, 1793

[28] Slane, P., Gaensler, B.M., Dame, T.M., Hughes, J.P., Plucinsky, P.P., Green, A. 1999, ApJ 525, 357

[29] Smith, R.C. 1997, AJ 114, 2667

[30] Tanaka, Y., Inoue, H., Holt, S.S. 1994 PASJ, 46, L37

[31] Tanimori, T., Hayami, Y., Kamei, S., Dazeley, S.A., Edwards, P.G., Gunji, S., Hara, S.Holder, J. et al. 1998, ApJ 497, L25

[32] Vink, J., Kaastra, J.S., Bleeker, J.A.M. 1997, A&A 328, 628

[33] Wentzel, D.G. 1974, ARA&A 12, 71

[34] Winkler, P.F.Jr. 1978, ApJ 221, 220